

LAND SURFACE
PROCESS/RADIOBRIGHTNESS MODELS
FOR NORTHERN PRAIRIE

by

Yuei-An Liou

A dissertation submitted in partial fulfillment
of the requirements for the degree of
Doctor of Philosophy
(Electrical Engineering and Atmospheric, Oceanic and Space Sciences)
in The University of Michigan
1996

Doctoral Committee:

Professor Anthony W. England, Co-Chair
Professor William R. Kuhn, Co-Chair
Professor Henry N. Pollack
Professor John F. Vesecky

RL-940 = RL-940

LAND SURFACE
PROCESS/RADIOBRIGHTNESS MODELS
FOR NORTHERN PRAIRIE

by

Yuei-An Liou

A dissertation submitted in partial fulfillment
of the requirements for the degree of
Doctor of Philosophy
(Electrical Engineering and Atmospheric, Oceanic and Space Sciences)
in The University of Michigan
1996

© Yuei-An Liou 1996
All Rights Reserved

To my mother, Mu-Tang Chang, my father, Ching-Chu, my wife, Shu-Yi, my
daughter, Alicia, and my family.

ACKNOWLEDGEMENTS

I thank my advisor, Prof. Anthony W. England, for his constant supervision, assistance, encouragement, and friendship during my graduate studies. Mere words can never describe my gratitude to him.

My graduate studies would not be complete without the support, help, and advice of the many professors and the many current and former fellow graduate students both with the Radiation Lab, Department of Electrical Engineering and Computer Science and with the Department of Atmospheric, Oceanic and Space Science (AOSS). I thank my committee members for their insightful comments and suggestions. In particular, I thank Prof. Bill Kuhn for his generous help when I enrolled in the Ph.D. Graduate Program in Electrical Engineering and AOSS. I also thank Dr. Richard Austin, Mr. Richard Carnes, Mr. Jui-Ching Cheng, Dr. Chen-Yu Chi, Mr. Tsen-Chieh Chiu, Mr. Craig Dobson, Mr. Mark Fischman, Ms. Natasha Flyer, Mr. Ed Kim, Dr. John Galantowicz, Ms. Jasmeet Judge, Dr. John Kendra, Dr. Joe Landry, Mr. Eric Li, Mr. Yi-Cheng Lin, Mr. Paul Siqueira, Dr. Jim Stiles, and Dr. Dong-Liang Wu for their technical advice and assistance, and friendship.

Finally, I would like to thank my wife, Shu-Yi, who has been my lasting support spiritually, and who has given me the joy and happiness of being a father of a lovely daughter, Alicia.

TABLE OF CONTENTS

DEDICATION		ii
ACKNOWLEDGEMENTS		iii
LIST OF TABLES		vi
LIST OF FIGURES		vii
LIST OF APPENDICES		x
CHAPTERS		
1	INTRODUCTION	1
1.1	Overview	1
1.2	Background	1
1.2.1	Soil Moisture	1
1.2.2	Biophysically-Based Models	3
1.2.3	Passive Microwave Remote Sensing	4
1.3	Format and Research Questions of the Thesis	5
2	The Annual Thermal/Radiobrightness (AT/R) MODEL	9
2.1	INTRODUCTION	10
2.2	THERMAL MODELS	12
2.2.1	Soil Constitutive Properties and Thermal Models	12
2.2.2	Boundary Conditions	15
2.2.3	Model Results	17
2.3	RADIOBRIGHTNESS MODEL	24
2.3.1	Soil Dielectric Properties and Radiobrightness Model	24
2.3.2	Model Results	30
2.4	DISCUSSION	35
3	The 1dH/R MODEL FOR BARE, UNFROZEN SOILS — A 1dHbu/R MODEL	37
3.1	INTRODUCTION	38
3.2	LAND SURFACE PROCESS MODEL	43
3.2.1	Governing Equations of Heat and Moisture Transfer	43

3.2.2	Finite Difference Scheme	46
3.2.3	Boundary Conditions	49
3.2.4	Hydraulic Conductivity and Water Retention	49
3.2.5	Liquid and Vapor Diffusivities	53
3.2.6	Simulation	55
3.3	Remote Measure of Soil Moisture	60
3.3.1	Soil Dielectric Properties	60
3.3.2	Soil Radiobrightnesses	61
3.3.3	RTI Measure of Soil Moisture	64
3.4	DISCUSSION	70
4	THE 1dH/R MODEL FOR BARE, FREEZING SOILS — A 1dHb/R MODEL	72
4.1	INTRODUCTION	73
4.2	HYDROLOGY MODEL	76
4.2.1	Governing Equations and Associated Terms	76
4.2.2	Temperature-Suction Relation	79
4.2.3	Numerical Scheme	80
4.2.4	Results	82
4.3	RADIOBRIGHTNESS MODEL	90
4.4	DISCUSSION	94
5	THE 1dH/R MODEL FOR PRAIRIE GRASSLAND	97
5.1	INTRODUCTION	98
5.2	THE GRASSLAND MODEL	100
5.2.1	Overview	100
5.2.2	The 1dH Module	102
5.2.3	The Radiobrightness Module	115
5.3	VALIDATION OF GRASSLAND MODEL	118
5.3.1	REBEX-1	118
5.3.2	Initial Conditions	119
5.3.3	Downwelling Longwave Radiation and Canopy Albedo	122
5.3.4	Comparing the Model to Observations	127
5.4	SIMULATION OF A 90-DAY DRY-DOWN	133
5.4.1	Thermal and Hydrologic Signatures	135
5.4.2	Radiobrightness	139
5.5	DISCUSSION	142
6	CONCLUSIONS	144
6.1	Contributions	144
6.2	Recommendations for Future Research	146
	APPENDICES	148
	BIBLIOGRAPHY	239

LIST OF TABLES

Table

2.1	Thermal conductivities, volumetric heat capacities, and densities of some soil materials, water, and air at 10°C and of ice at 0°C (after de Vries [24]).	15
2.2	The differences between the maximum and minimum surface temperatures over an annual cycle at four times for 17 % and 38 % moist soils.	24
2.3	Parameters required for computing radiometric properties of the soil-water system.	27
3.1	Change in the diurnal average radiobrightness over the 60-day simulation for both water transport and no water transport cases at 19, 37 and 85 GHz horizontal polarization.	64
3.2	Diurnal variations in radiobrightness between 2 p.m. and 2 a.m. for both water transport and no water transport cases at 19, 37 and 85 GHz horizontal polarization.	64
4.1	The maximum and minimum of T_b (water transport) - T_b (no water transport) for 19 GHz, horizontal polarization.	94
5.1	Observations of LAI for a variety of vegetation.	121
5.2	The AD and SD from comparisons between the model-predicted $Q_{1,d}$ and reference case 1 (Equation (5.44) with albedo = 0.1).	127
5.3	The AD and SD from comparisons between the model-predicted $Q_{1,d}$ and reference case 2 (Equation (5.44) with albedo = 0.4).	127
5.4	The AD and SD based upon comparisons between measured- and predicted-soil temperatures at 2, 4, 8, 16, 32, and 64 cm depths. . .	130
6.1	Summary of the inputs, forcings, and products of the four models presented in the dissertation. The notations are: $T_g(z)$, soil temperature profile; $\theta(z)$, soil moisture profile; Q_{1h} , latent heat transfer; Q_{sh} , sensible heat transfer; T_c , canopy temperature; θ_c , canopy moisture; Q_g , thermal emission from the terrain; and T_b , terrain radiobrightness. . .	144

LIST OF FIGURES

Figure

2.1	(a) Unfrozen water content. (b) Apparent volumetric heat capacity. (c) Thermal conductivity. These soil constitutive properties are applied to both diurnal and annual models.	14
2.2	Diurnal surface temperatures for (a) 17 % with latent heat transfer, (b) 38 % moist soils with latent heat transfer, and (c) 38 % moist soils without latent heat transfer for 03/22, 06/22, 09/22 and 12/22. . . .	19
2.3	38 % moist soil isotherms with latent heat transfer for 03/22 and 06/22.	21
2.4	17 % moist soil isotherms with latent heat transfer for 03/22 and 06/22.	22
2.5	38 % moist soil isotherms without latent heat transfer for 03/22 and 06/22.	23
2.6	Differences in diurnal surface temperatures between annual and diurnal models for (a) 17 % moist soil and (b) 38 % moist soil for 03/22, 06/22, 09/22 and 12/22.	25
2.7	Annual surface temperature variations at four times: 2 a.m., 6 a.m., 2 p.m., and 6 p.m. for (a) 17 % moist soil and (b) 38 % moist soil. . .	26
2.8	Dielectric constants of (a) 17 % moist soil and (b) 38 % moist soil at 19, 37 and 85 GHz.	29
2.9	Emissivity versus temperature at the 53° angle of incidence of the SSM/I for (a) 17 % moist soil and (b) 38 % moist soil.	31
2.10	Diurnal maxima and minima of the first-order terms for (a) vertical polarization and (b) horizontal polarization for 17 % moist soil. . . .	32
2.11	Semiannual radiobrightness signatures for (a) 19 GHz horizontal polarization, and (b) 37 GHz horizontal polarization for 17 % moist soil.	34
2.12	Semiannual radiobrightness signatures for (a) 19 GHz horizontal polarization, and (b) 37 GHz horizontal polarization for 38 % moist soil.	36
3.1	(a) Schematic diagram for the soil layers. (b) Flowchart of 1dHu model algorithm.	47
3.2	(a) Soil water retention for the Salkum silt loam. (b) Hydraulic conductivity as a function of moisture content.	52
3.3	(a) Thermal liquid and vapor diffusivities. (b) Isothermal liquid and vapor diffusivities.	56

3.4	(a) Soil moisture content at the surface for the water transport and no water transport cases. (b) Soil moisture profile for the water transport case.	57
3.5	(a) Surface temperature for the water transport case. (b) Differences in surface temperatures between the water transport and no water transport cases.	59
3.6	Soil temperature profile on 06/22 for the water transport case. . . .	60
3.7	(a) Complex relative permittivities of soil at the surface conditions of the water transport case. (b) Emissivities associated with (a).	62
3.8	Radiobrightness signatures for 19 GHz horizontal polarization (a) for the water transport case, and (b) for the no water transport case. . . .	65
3.9	(a) Soil moisture content at the surface at four times: 2 a.m., 6 a.m., 2 p.m., and 6 p.m. for the 38 %, 24 %, and 17 % cases (all with water movement in the soil). (b) Surface temperature at four times: 2 a.m., 6 a.m., 2 p.m., and 6 p.m. for the 38 %, 24 %, and 17 % cases.	68
3.10	(a) Radiobrightness differences between 2 p.m. and 2 a.m. for the 38 %, 24 %, and 17 % cases. (b) Radiobrightness differences between 6 p.m. and 6 a.m. for the 38 %, 24 %, and 17 % cases.	69
4.1	Flowchart of the 1dHb model algorithm for freezing soils. “NRM” denotes the Newton-Raphson Method.	81
4.2	(a) Temperature and (b) liquid water and ice contents at the surface for the water transport case.	83
4.3	(a) Temperature, (b) liquid water content, and (c) ice content profiles over a diurnal cycle on day 19. Sunrise occurs at 7:10 a.m. with a peak insolation of 360 W/m ² at 12:10 p.m.. The sun sets at 5:20 p.m. Note the change in vertical scales from 40 cm in (a) to 5 cm in (b) and (c).	85
4.4	(a) Temperature, (b) liquid water content, and (c) ice content profiles over a diurnal cycle on day 60. Sunrise occurs at 7:20 a.m. with a peak insolation of 290 W/m ² at 12:10 p.m. The sun sets at 5 p.m.	88
4.5	(a) Temperature, (b) liquid water content, and (c) ice content profiles for the water transport case. Note that the depth scale of (c) differs from that of (a) and (b).	89
4.6	Differences in (a) liquid and ice contents and in (b) temperature at the surface between the water transport and no water transport cases. . . .	91
4.7	Surface temperatures on (a) day 19, (b) day 44, and (c) day 60. Liquid water and ice contents on (d) day 19, (e) day 44, and (f) day 60. . . .	92
4.8	(a) H-polarized, 19 GHz radiobrightness for the water transport case. (b) Differences in H-polarized, 19 GHz radiobrightness between the water transport and no water transport cases.	95
5.1	Schematic diagram of the 1dH/R model inputs and products.	101
5.2	The 1dH module schematic diagram of land-air interactions for vegetated fields.	103
5.3	Radiobrightness components of the 1dH/R model.	118

5.4	Predicted $Q_{1,d}$ using the current proposed approach and the models proposed by Brutsaert [1975], Satterlund [1979], and Kahle [1977].	125
5.5	(a) Measured canopy and air temperatures, and predicted canopy temperature. (b) Measured and predicted soil heat fluxes at 2 cm depth.	128
5.6	Soil temperatures at 2, 4, 8, 16, 32, and 64 cm depths.	131
5.7	1.4, 19, and 37 GHz horizontally polarized radiobrightnesses.	132
5.8	(a) Soil moisture content at the surface for the prairie and bare soil cases. (b) Soil moisture profile for the bare soil case. (c) Soil moisture profile for the prairie case.	134
5.9	(a) Surface temperature for the prairie case. (b) Difference in surface temperatures between the prairie and bare soil cases.	136
5.10	Soil temperature profiles on 06/22 (a) for the bare soil case and (b) for the prairie case.	137
5.11	Temperature for the canopy, thatch, and surface on day 201.	138
5.12	Horizontally polarized radiobrightnesses at 1.4 , 19 and 37 GHz (a) versus daynumber and (b) versus soil moisture for the prairie case. (c) The percentage of radiobrightness contributed by the soil.	140
5.13	Differences in radiobrightness between 2 p.m. and 2 a.m. versus soil moisture for both the bare soil and prairie cases.	141

LIST OF APPENDICES

APPENDIX

A	THE AT/R MODEL	149
B	THE 1dH/R MODEL	184

CHAPTER 1

INTRODUCTION

1.1 Overview

In this dissertation, I use four numerical models to examine the sensitivity of radiobrightness to soil moisture in bare and grass-covered prairie soils. These models are: an Annual Thermal/Radiobrightness (AT/R) model for freezing soils (Chapter 2); a one-dimensional Hydrology/Radiobrightness (1dH/R) model for bare, unfrozen soils (a 1dHbu/R model — Chapter 3); a 1dH/R model for bare, freezing soils (a 1dHb/R model — Chapter 4); and a 1dH/R model for a prairie grassland (Chapter 5). Each successive model involves increasing complexity. I present a chapter on each model describing the added complexity and its consequences. The FORTRAN computer codes for the AT/R model and a 1dH/R model of mixed bare and grass-covered soils are included in Appendices A and B, respectively.

1.2 Background

1.2.1 Soil Moisture

Moisture plays a crucial role in the land-atmosphere energy balance because it governs the partitioning of energy and water through evaporation and transpiration at the lower boundary of the atmosphere. Considerable effort has been made to understand the effects of soil moisture on atmospheric circulation. For example,

Namias [83] was among the first to address the influence of anomalous soil moisture conditions on the atmosphere. Because he and others found that seasonal anomalies of soil wetness had a significant effect on the atmospheric seasonal cycles, models of energy and moisture transfer in soil and vegetation that lead to estimates of land-air energy fluxes must be accurate if the predictions of atmospheric circulation models are to be reliable.

Energy and moisture transfer in soil were successfully described by Philip and de Vries [92] and de Vries [23]. In their theory, energy and moisture movement are coupled through temperature gradients, liquid water concentration gradients, pressure gradients, and gravity. The theory has been used by Milly and Eagleson [79, 80], Milly [77, 78], Abdel-Hadi and Mitchell [1], Shah et al [107], Thomas [114], Ewen and Thomas [34], and Thomas and King [115]. Its weaknesses are relatively well understood by the soil science community, and it continues to be the best theory available.

Freezing soils exhibit a very different coupled transfer of energy and moisture from that of non-freezing soils. The differences are associated with the following four respects: 1) liquid water and ice co-exist over a wide range of temperatures below the freezing depression point (FDP) [127, 4, 36, 116, 90, 12]; 2) liquid water content becomes the iterative solution of highly nonlinear, coupled temperature-suction and water-retention equations; 3) temperature-moisture content curves for repeatedly freezing and thawing soils exhibit hysteresis [64, 50]; and 4) ice lensing and frost heaving occur as liquid water is drawn to the freezing front [5, 42, 16, 63].

In vegetated areas, moisture available to the atmosphere is from both the wetted foliage through evaporation and the dry foliage through transpiration [25, 106, 130]. Transpired water is affected by the incoming solar radiation, air vapor pressure deficit,

soil moisture (matric head), and air temperature [86]. Among these factors, soil moisture determines the maximum rate of water that can be extracted from the root zone. In this manner, soil moisture regulates the exchanges of energy and moisture fluxes at the land-air interface.

1.2.2 Biophysically-Based Models

Many researchers over the past few years have attempted to develop biophysically-based models that predict vertical moisture and temperature profiles of soil and vegetation as well as surface fluxes. Two of the most comprehensive ones are BATS [25] and the Simple Biosphere model (SiB) [106]. They possess three common features. First, both are designed for use in general circulation models (GCMs). Second, they consider a broad range of soil textures whose thermal and hydraulic properties are specifically prescribed. Third, land cover is modeled biophysically and realistically to compute the albedo, drag, and energy partitioning characteristics of the associated vegetated surface.

The two models were applied in a variety of studies related to weather and climate. First, Dickinson and Henderson-Sellers [26] incorporated the BATS model into the NCAR Community Climate Model (CCM) to study the effects of tropical deforestation on climate. They replaced the Amazon tropical forest in South America with impoverished grassland and ran a 13-month simulation. The results were compared with those obtained from the original CCM. They found that reduced sensible heat exchange and less interception and evaporation from the canopy caused runoff to increase and surface temperatures to rise by 3 to 5 K. This had a detrimental impact on the survival of the remaining forest and on attempts at cultivation in deforested areas. Second, Sato et al [103] implemented SiB in a modified version of the

National Meteorological Center’s global spectral GCM (SiB-GCM). Their motivation was to investigate the effect of replacing the conventional bucket hydrology model of Manabe [75] with SiB of Sellers et al [106] and Dorman and Sellers [28]. The study showed that the SiB-GCM produced a more realistic partitioning of energy at the land surface than the conventional GCM.

In summary, it has been recognized that the inclusion of more biophysically realistic parameterizations of land surface processes leads to better GCM performance [26, 103]. The degree of parameterization should be carefully balanced between computational economy and model performance.

1.2.3 Passive Microwave Remote Sensing

Satellites that are designed for frequent coverage of the land surface are particularly useful in inferring land-surface parameters and fluxes. In particular, microwave frequencies are sensitive to soil moisture through the dominant influence of liquid water upon microwave emissivity in bare or sparsely vegetated soils [19, 87, 88, 3]. Dense vegetation becomes the physical link between the soil and the atmosphere and absorption and scattering of microwave energy in a dense canopy can dramatically decrease the sensitivity of radiobrightness to soil moisture, especially at higher microwave frequencies. In general, lower-frequencies are preferred for their sensitivity to soil moisture with L-band being the best [105].

Microwave frequencies are sensitive to the state and amount of soil moisture because of a significant contrast in the relative dielectric permittivity between liquid water and ice as described by the Debye relaxation equation [119]. The relaxation frequency of liquid water lies in the microwave band, while that of ice lies in the kilohertz band. Since moisture content and state dominate soil dielectric properties

(i.e., the radiometric behaviors of frozen and thawed soils are very different), it is possible to classify frozen and thawed soils using radiobrightness. For example, a combination of the 37 GHz radiobrightness and the 10.7 to 37 GHz spectral gradient from the Scanning Multichannel Microwave Radiometer (SMMR) has been used to map the freeze/thaw boundaries in the upper Midwest of the United States for the fall of 1984 [131, 132].

1.3 Format and Research Questions of the Thesis

The overall objective of the thesis is to link the moisture stored in bare and grass-covered prairie soils to radiobrightness. Because radiobrightness is sensitive only to moisture in the upper few centimeters of soil [33], the linkage to relevant moisture stored in the upper meter of soil requires a model of moisture transport in the soil, i.e., 1dH models. The thesis is organized according to increasing complexity of these models.

Chapter 2 introduces the AT/R model. The AT module focuses upon physical treatments of soil to track energy transfer for estimates of the temporal soil temperature profile. Thermal properties such as apparent volumetric heat capacity [6] and thermal conductivity [24] are functions of temperature — particularly at freezing temperatures in moist soils. These temperature dependences render the heat flow equation highly nonlinear, especially as free water freezes or thaws and as phase boundaries propagate. The depressed freezing point (DFP) is determined using the approach of Andersland et al [6]. I solved the one-dimensional heat flow equation using the finite element scheme of England [29] which tracks isotherms within the soil.

Results from the AT module are linked to an R module for predictions of annual

radiobrightnesses. Wet soils are sufficiently absorptive of microwaves that effective emission depths are usually less than a few centimeters. This permits a first-order approximation to the radiobrightnesses of bare, quasi-specular, wet soils [29, 69]. At temperatures above the DFP, soil dielectric properties are estimated from a four-component mixture of soil solids, air, free water, and bound water [27, 119]. Below the DFP, ice becomes a 5th component. Fresnel coefficients are used to estimate reflectivities. To demonstrate the significance of seasonal weather forcing upon thermal and radiobrightness signatures, I compare the predictions from the AT/R model with those of an equivalent diurnal thermal/radiobrightness model.

The 1dHbu/R model for bare, unfrozen soils is described in Chapter 3. Unlike the AT/R model, energy and moisture transport are coupled through theory of Philip and de Vries [92, 23]. A finite difference scheme is used to solve these coupled equations to obtain the temperature and moisture profiles in the soil. At the upper boundary of the soil column, the Newton-Raphson method [94] is applied to match energy and moisture fluxes. At the lower boundary, constant energy fluxes are obtained from the AT module results. The hydraulic conductivity of the moist soil follows the Mualem model [82]. The corresponding water-retention relation follows the two-parameter junction model of Rossi and Nimmo [102]. I also incorporate improved models for the vapor diffusion coefficients [61] and the tortuosity factor for the diffusion of gases in soil [66].

The thermal module is linked to an R module as in the AT/R model. I simulate a 60-day dry-down of bare, unfrozen soils in summer to examine the relative influence of moisture movement on radiobrightness. I also re-examine the Radiobrightness Thermal Inertia (RTI) [31] measure of soil moisture for bare soil. RTI relates soil moisture to the diurnal variation in radiobrightness through the increase in thermal

inertia and the decrease in emissivity with increasing moisture content.

Chapter 4 concerns the 1dHb/R model for bare, freezing soils. The 1dHb module is an improved version of the 1dHbu module that accounts for soil freezing and thawing. Using the 1dHb/R model, I ran a 90-day, northern latitude, fall/winter, dry-down simulation to examine the influence of water transport on the soil temperature, moisture, and radiobrightness signatures of bare, freezing soils.

Chapter 5 concerns the 1dH/R model for prairie grassland. The 1dH module simulates the land surface processes and estimates the temporal temperature and moisture profiles in the soil and canopy for a prairie grassland. The treatment of the soil is similar to that in the 1dHb and 1dHbu modules except that I also account for the influence of transpiration on the coupled energy and moisture transfer within the root zone. The grass canopy is regarded as a one-layer biophysical medium with dynamic energy and moisture exchanges with the soil and with the atmosphere. The grass cover may vary from 0 % to 100 %. Sensible heat transfer is determined using the bulk aerodynamic approach [117]. The aerodynamic resistance is given by Chehbouni et al [18]. Latent heat transfer by evaporation from bare soil or wet foliage is modeled in a fashion similar to the sensible heat transfer. Latent heat transfer due to transpiration is treated using the approach of Verseghy et al [123]. In this approach, the latent heat transfer is affected by foliage temperature, water potential, insolation, soil temperature, and moisture content/state. The Newton-Raphson method is applied to match the boundary energy and moisture fluxes at the soil-canopy interface. Thatch is included as an insulating layer that is subject only to radiation exchange with the overlying canopy and the underlying soil.

Temperature and moisture profiles from the 1dH module are incorporated into the R module to estimate radiobrightness. The R module and its associated dielectric

properties are similar to the radiative transfer model of England and Galantowicz [32]. The total model brightness is comprised of the soil brightness attenuated by one trip through the canopy, the downwelling canopy brightness reflected by the soil and attenuated by one trip through the canopy, the upwelling canopy brightness, and the sky brightness reflected by the soil and attenuated by two trips through the canopy. The relative permittivity of the wet canopy is approximated by the dual-dispersion model of Ulaby and El-Rayes [120]. The optical thickness of the grass layer is from England and Galantowicz [32].

Predictions from the 1dH/R model are compared with observations from the First Radiobrightness Energy Balance Experiment (REBEX-1) on prairie grassland near Sioux Falls, South Dakota, during the fall and winter of 1992-1993 [39]. The comparisons include soil heat flux at 2 cm depth, soil temperatures at 2, 4, 8, 16, 32, and 64 cm depths, canopy temperature, and horizontally polarized radiobrightnesses at 19 and 37 GHz.

Upon verifying the 1dH/R model, I ran the model for a 60-day dry-down simulation for a 100 % vegetation-covered prairie in summer to study the sensitivity of radiobrightness to soil moisture. The utility of the RTI measure of soil moisture in vegetated fields is also examined.

Chapter 6 is a summary that includes the major contributions of the thesis and recommendations for future research.

CHAPTER 2

The Annual Thermal/Radiobrightness (AT/R) MODEL

Abstract — We have developed physically based, diurnal and annual models for freezing/thawing moist soils subject to annual insolation, radiant heating and cooling, and sensible and latent heat exchanges with the atmosphere. Both models have the same weather forcing, numerical scheme, and soil constitutive properties. We find that surface temperature differences over a diurnal cycle between the annual and diurnal models are as much as -5 Kelvins in March, -7 Kelvins in June, -4 Kelvins in September, and 5 Kelvins in December for 38 % (by volume fraction) moist soil. This difference occurs because the annual model includes the history of energy fluxes at the surface of the soil.

The annual model is linked to microwave emission models for predictions of temporal radiobrightness signatures. The model predicts a relatively weak decrease in diurnal differences in soil temperature with increased moisture content, but a significant decrease in diurnal differences in radiobrightness. It also exhibits notable perturbations in radiobrightness when soils freeze and thaw. The moisture dependent, day-to-night radiobrightness difference is enhanced by as much as -42 Kelvins at 19.35

GHz horizontal polarization for frozen soil if daytime thawing occurs.

2.1 INTRODUCTION

Land surface processes strongly influence the dynamics of the atmosphere over a wide range of space and time scales through exchanges of momentum, moisture, and energy. Soil surface temperature and moisture are key parameters in that they are products of the energy balance between the land and atmosphere. They are also diagnostic parameters in that they govern infrared and microwave emission. Reliably modeling soil surface temperature and moisture are crucial to simulate land-atmosphere interactions and to study radiometric signatures of bare or sparsely vegetated soil.

The focus of this paper is upon the radiobrightness of moist agricultural soils in northern prairie during periods when they are bare of vegetation. Such conditions exist over significant periods of a year for many fields in the northern Great Plains and on the steppes of Asia. None of these fields will fill a resolution cell of a satellite sensor such as the Special Sensor Microwave/Imagers (SSM/I) which have spatial resolutions of 69×43 km at 19.35 GHz, 37×28 km at 37.0 GHz, and 15×13 km at 85.5 GHz [49].

One strategy for synthesizing an expected radiobrightness for a resolution cell would be to aggregate the predicted radiobrightnesses of typical landcover types for the cell according to their expected occurrence throughout an annual cycle. The bare field, or one that is covered by stubble, would be an expected occurrence in agricultural prairie – especially during spring and fall when hydrologists would particularly like to know the quantity of water that is stored in soil or snow. Our overarching objective in this and a companion paper (Chapter 3) [71] is to develop an expected annual radiobrightness for these bare soils.

Several one-dimensional thermal models have been developed for bare rocks or soils to predict their thermal infrared (TIR) or thermal microwave (radiobrightness) signatures over diurnal periods. Watson [125] applied the Laplace transform method to develop a diurnal model for rock and dry soils. He proposed using diurnal temperature extremes – a measure of a rock’s thermal inertia – to discriminate among rock types in TIR images. Kahle [59] developed a diurnal finite difference model for moist soils and proposed using thermal inertia to discriminate among various soils. Price [95, 96] developed a similar model and demonstrated that thermal inertia could be used to infer soil moisture. England [29] developed a diurnal finite element model for freezing and thawing soils to examine the empirical observation that a combination of 10 and 37 GHz radiobrightness from the Scanning Multichannel Microwave Radiometer (SMMR) could be used to map frozen and thawed prairie soils [30], and to extend the TIR-based, thermal inertia technique of estimating soil moisture to the SSM/I’s spectral range of 19-85 GHz [31].

None of these diurnal models, nor any of the more recent remote sensing thermal models for vegetation covered terrains, place the diurnal thermal event in an annual context, nor do they incorporate physical models of freezing point depression or of coupled thermal and moisture transport. Using a variable time interval Laplace method to create an annual model for dry soils, Liou and England [69] found significant differences in predicted surface temperatures between the annual model and an equivalent diurnal model. Because soil temperature is a convolution of many past diurnal events, the seasonal history is embedded in the surface temperature. In our companion paper (Chapter 3) [71], we report on a finite difference, coupled temperature and moisture, diurnal radiobrightness model based upon the thermal modeling approach of de Vries [24] and advanced by Milly and others [79, 80, 77, 15, 78, 7].

However, this coupled model is too computationally intensive to become a practical annual model.

In this paper, we present the finite element annual thermal/radiobrightness model for moist soils that are subject to freezing and thawing, and compare the model's predictions with those of our equivalent diurnal model [29]. Our specific objectives are to extend our earlier findings for dry soils [69] to the more interesting case of the moist, freezing and thawing soils found in northern prairie; and to identify appropriate lower boundary temperatures by latitude and day-of-year for use as lower boundary temperatures in our coupled model for bare, moist soils (Chapter 3) [71]. The use of this lower boundary temperature places the coupled diurnal model in the approximate thermal context of an annual model. We also achieve a more rapid convergence of the coupled model by initializing its temperature profile with the temperature profile from this annual model for latitude and day-of-year.

2.2 THERMAL MODELS

2.2.1 Soil Constitutive Properties and Thermal Models

Soil temperatures are obtained by solving the one-dimensional heat flow equation within soil:

$$\frac{\partial}{\partial t} (C_p(T_g) \cdot T_g(z, t)) = \frac{\partial}{\partial z} \left(\lambda(T_g) \cdot \frac{\partial T_g(z, t)}{\partial z} \right), \quad (2.1)$$

where C_p is the apparent volumetric heat capacity of the soil at constant pressure ($\text{J}/\text{m}^3\text{-K}$), $T_g(z, t)$ is the ground temperature at depth z (m) and time t (s), and λ is the thermal conductivity ($\text{W}/\text{m-K}$). Following Andersland et al [6], the apparent volumetric heat capacity is described by

$$C_p = C_d + C_i(\theta - \theta_u) + C_u\theta_u + L_f \frac{\partial \theta_u}{\partial T}, \quad (2.2)$$

where C_d is the volumetric heat capacity of dry soil matrix, C_i is the volumetric heat capacity of ice, C_u is the volumetric heat capacity of unfrozen water, θ is the total water content, (m^3/m^3), θ_u is the unfrozen water content, and L_f is the volumetric latent heat of fusion (J/m^3). Soil thermal conductivity is computed by using the de Vries' model [24]:

$$\lambda = \frac{\sum_{i=1}^n k_i \theta_i \lambda_i}{\sum_{i=1}^n k_i \theta_i}, \quad (2.3)$$

where $k_i, i = 1, \dots, n$ is the weighting function of the i^{th} constituent; $\theta_i, i = 1, \dots, n$ is the volumetric content of the i^{th} constituent; and $\lambda_i, i = 1, \dots, n$ is the thermal conductivity of the i^{th} constituent.

Figure 2.1 shows the apparent volumetric heat capacity, unfrozen water content and thermal conductivity of 17 % and 38 % (by volume fraction) moist soils versus temperature.

Figure 2.1 (a) indicates that unfrozen water content decreases exponentially with decreasing temperature below the depressed freezing point (DFP) [6] and the rate of decrease depends upon soil texture. In general, the lower the moisture content, the lower the DFP. The DFP is 267.2 K for 17 % moist soil and 272.5 K for 38 % moist soils. In this paper, we chose a silt loam because it is typical of prairie soils. Typical silt loams have a porosity, field capacity and wilting point of 48 %, 28.6 %, and 13.3 %, respectively. Their dry substance consists of 19 % sand, 22.5 % clay, and 58.5 % silt [102]. Soil constituents, water, ice, and air have very different thermal properties as shown in Table 1. Figure 2.1 (b) shows that moist soils have an extremely high heat capacity as moisture begins to freeze at temperatures slightly lower than the DFP. Figure 2.1 (c) shows that soils with a higher moisture content have a higher thermal conductivity below the DFP, while those with a lower moisture content behaves weakly in the opposite sense.

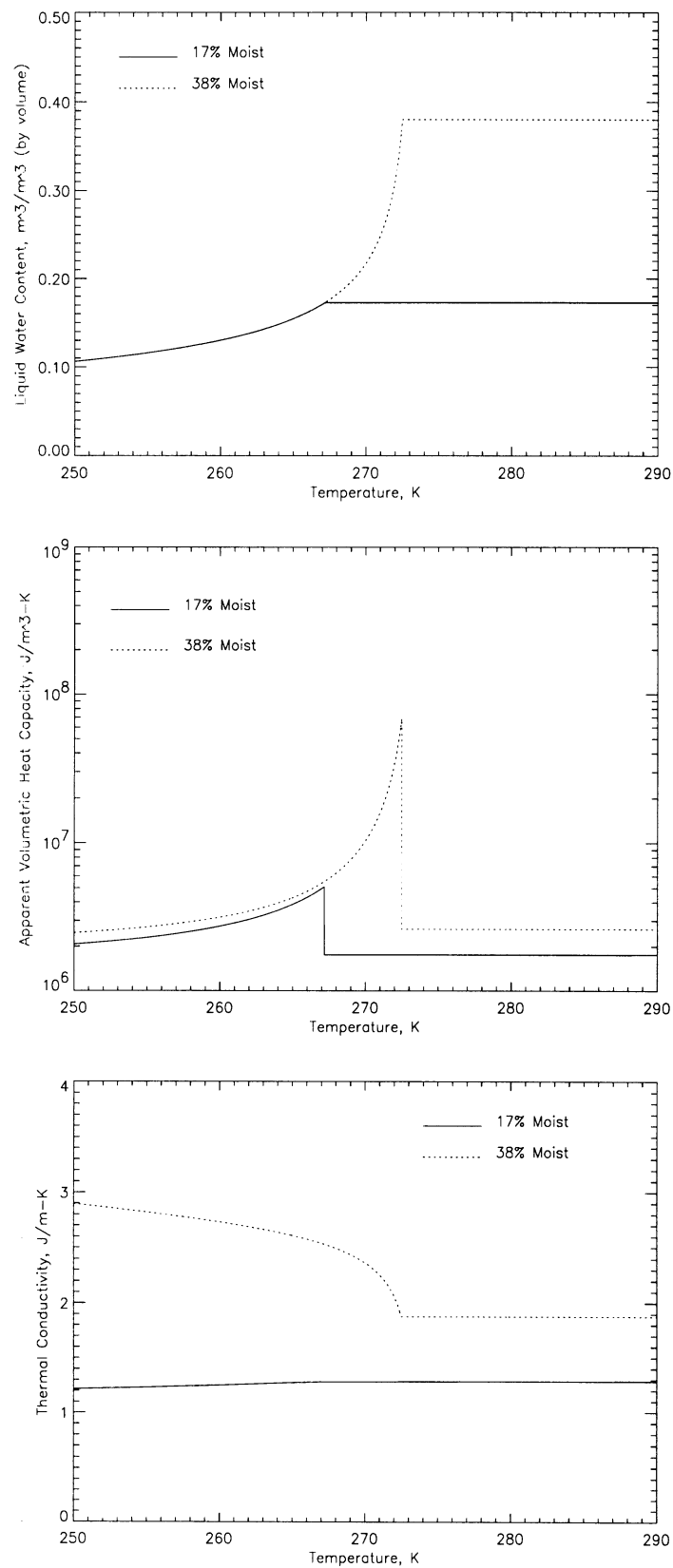


Figure 2.1: (a) Unfrozen water content. (b) Apparent volumetric heat capacity. (c) Thermal conductivity. These soil constitutive properties are applied to both diurnal and annual models.

Substance	λ , W/m-K	C , J/m ³ -K	ρ , kg/m ³
Quartz	8.892	2.009×10^6	2660
Clay	2.930	1.894×10^6	2650
Water	0.586	4.194×10^6	1000
Ice	2.240	1.937×10^6	917
air	0.249	1.237×10^3	1.231

Table 2.1: Thermal conductivities, volumetric heat capacities, and densities of some soil materials, water, and air at 10°C and of ice at 0°C (after de Vries [24]).

C_p and λ are an aggregate of the physical properties of all of the soil constituents. Because some of these are temperature dependent, the heat flow equation is highly nonlinear with soil temperature. The problem becomes particularly difficult as the state of free water within soil changes and phase boundaries propagate. To solve (2.1), we used the finite element scheme of England’s model [29] which tracks isotherms within the soil.

The term in parenthesis on the right of equation (2.1) is the negative of the energy flux at depth z and time t . Equation (2.1) is solved by imposing the following boundary conditions of weather forcing at the land-atmosphere interface and a zero energy flux at a depth beyond the annual thermal pulses.

2.2.2 Boundary Conditions

The energy budget at the land–atmosphere interface is a balance among radiant heat, sensible heat, and latent heat. The energy flux available to soil at the surface is

$$F(0, t) = F_{\text{sun}}(t) + F_{\text{sky}}(t) - F_{\text{sh}}(t) - F_{\text{lh}}(t) - F_{\text{g}}(t), \quad (2.4)$$

where F_{sun} is insolation reduced by cloud extinction, atmospheric absorption, albedo, and the cosine of the zenith angle; F_{sky} is sky brightness with a correction for cloud cover; F_{sh} is the sensible heat transfer from the land to the atmosphere; F_{lh} is the

latent heat transfer from the land to the atmosphere; and F_g is gray-body emission from the soil's surface. F_{sun} , F_{sky} and F_g have been further described in England [29]. The sensible heat transfer from the bulk transfer method may be expressed by [117]

$$F_{\text{sh}} = \rho_a \cdot c_{p, a} \cdot \left(\frac{T_g(0, t) - T_a(z_r, t)}{r_a} \right), \quad (2.5)$$

where r_a is the aerodynamic resistance (s/m), ρ_a is the air density (kg/m³), $c_{p, a}$ is the air specific heat at constant pressure (J/kg-K), $T_a(z_r, t)$ is the air temperature at a reference height z_r and time t (K). The latent heat transfer is given by [91]

$$F_{\text{lh}} = f \cdot \frac{F_{\text{sh}}}{B}, \quad (2.6)$$

where f is evaporation efficiency, and B is the Bowen ratio. The evaporation efficiency, a ratio between real evaporation and potential evaporation, is chosen to be a linear function of soil moisture content with values between 0 and 1 corresponding to wilting point and saturation, respectively.

The Bowen ratio may be estimated by [91]

$$B = \gamma \cdot \frac{T_a(0, t) - T_a(z_r, t)}{e(0, t) - e(z_r, t)}, \quad (2.7)$$

where γ is the psychrometric constant (Pa/K), $e(0, t)$ is surface water vapor pressure (Pa), and $e(z_r, t)$ is air vapor pressure at the reference height (Pa). Air temperature is assumed to be the climatic value for the time-of-day and day-of-year of the location for which the model was run. For our purposes, this location was chosen to be Sioux Falls, South Dakota. The partial pressure of the water vapor was arbitrarily chosen to be constant through a day and of a value that would yield a 40 % humidity at solar noon. The psychrometric constant is expressed as [91]

$$\gamma = \frac{c_{p, a} \cdot p}{0.622 \cdot L_e}, \quad (2.8)$$

where p is the atmospheric pressure at the boundary layer (Pa), and L_e is the latent heat of evaporation of water (J/kg).

The saturation water vapor pressure is obtained by solving

$$\log(0.01e) = 9.4041 - \frac{2354}{T}, \quad (2.9)$$

where \log is decimal logarithm, and T is the temperature. Equation (2.9) is from the Clausius–Clapeyron equation with higher–order terms neglected [53].

2.2.3 Model Results

The ground warms quickly as the sun rises. Capturing these rapid changes with the numerical integrations requires time intervals of 10 minutes or less. Because there are over fifty thousand 10–minute intervals in an annual cycle, compared to only 144 intervals in a diurnal cycle, the numerical simulation of the annual model becomes computationally intensive. To gain quicker convergence, the annual equilibrium temperature (AET) is assigned as the initial temperature of soil at all depths and all time-steps. The AET is chosen so that the sum of incoming absorbed insolation and sky radiation and the outgoing emission from the surface are in balance. A similar treatment for the initial temperature is applied to the diurnal model.

The annual temperature at all depths and all time-steps generally differs from AET by less than 40 Kelvins so that its profile can be sufficiently described by 40 dynamic one-Kelvin isotherms. Similarly, 20 one-Kelvin isotherms are generally sufficient for a diurnal model. The actual number of isotherms is not only dependent upon time scale, but also dependent upon moisture content and state.

Figure 2.2 shows the surface temperatures for 17 % moist soil with latent heat transfer, and 38 % moist soil with and without latent heat transfer for March, June,

September, and December at a northern latitude of 43.5 degrees (that of Sioux Falls, South Dakota). Soils appear to resist changes in temperature as moisture freezes and thaws (Figure 2.2 for dates 03/22 and 12/22). A comparison of Figure 2.2 (a) and (b) shows 17 % moist soils respond to the weather forcing at the land-atmosphere interface faster and to a greater extent than to the 38 % moist soils, i.e., wetter soils have a higher apparent thermal inertia. The difference in the diurnal variation is 7.8 Kelvins for March, 6.8 Kelvins for June, 5.4 Kelvins for September, and 5.2 Kelvins for December. A comparison between Figure 2.2 (b) and (c) shows that latent heat exchanges with the atmosphere tend to suppress diurnal temperature variation. These decreases are 1 Kelvin for March, 4.4 Kelvins for June, 2.8 Kelvins for September, and 0.01 Kelvins for December. The decreases are in the direction to enhance the effect of moisture on apparent thermal inertia.

The thermal conductivity of 38 % moist soil is more than two times larger than that of 17 % moist soil at temperatures below the DFP so that the apparent thermal inertia is greater in March and December for more moist soils (Figure 2.1 (c)). More importantly, apparent volumetric heat capacity of 38 % moist soil is more than an order of magnitude greater than that of 17 % moist soil at temperatures between their DFPs (Figure 2.1 (b)).

Figure 2.3 shows the diurnal isotherms for 38 % moist soil with latent heat transfer for March and June. Notable characteristics include (1) isotherms are created after sunrise and start to merge some time after peak insolation; (2) temperature gradients in the first few centimeters are much larger during the day than during the night; (3) soil temperatures at depths below 0.8 meter remain approximately constant during a diurnal cycle; and (4) diurnal thermal pulses penetrate approximately 50 cm in June but less than 20 cm in March when a large fraction of the insolation is used to melt

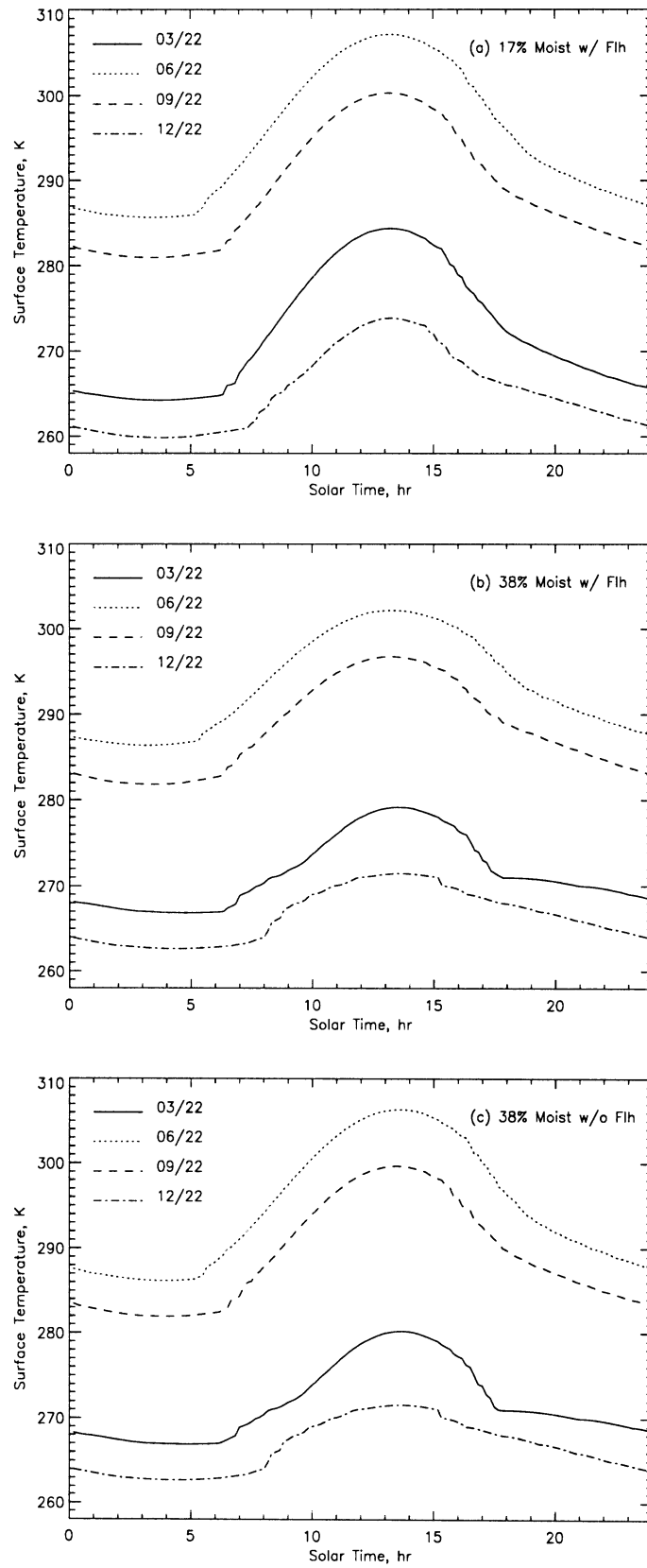


Figure 2.2: Diurnal surface temperatures for (a) 17 % with latent heat transfer, (b) 38 % moist soils with latent heat transfer, and (c) 38 % moist soils without latent heat transfer for 03/22, 06/22, 09/22 and 12/22.